Photophysical and cellular imaging studies of brightly luminescent osmium(II) pyridyltriazole complexes

Salem A. E. Omar,[a,b] Paul A. Scattergood,[a,b] Luke K. McKenzie,[c,d] Callum Jones,[c] Nathan J. Patmore,[a] Anthony J. H. M. Meijer,[d] Julia A. Weinstein,[d] Craig R. Rice,[a] Helen E. Bryant[c]* and Paul I. P. Elliott[a,b]*

a Department of Chemistry, University of Huddersfield, Queensgate, Huddersfield, HD1 3DH, UK

b Institute of Molecular Medicine, University of Huddersfield, Queensgate, Huddersfield, HD1 3DH, UK

c Academic Unit of Molecular Oncology, Sheffield Institute for Nucleic Acids (SInFoNiA), Department of Oncology and Metabolism, University of Sheffield, Beech Hill Road, Sheffield, S10 2RX, UK

d Department of Chemistry, University of Sheffield, Brook Hill, Sheffield, S3 7HF, UK

** corresponding author: p.i.elliott@hud.ac.uk; h.bryant@sheffield.ac.uk*

Abstract: The series of complexes $[Os(bpy)_{3-n}(pytz)_n][PF_6]_2$ (bpy = 2,2'-bipyridyl, pytz = 1-benzyl-4-(pyrid-2-yl)-1,2,3-triazole, **1** n = 0, **2** n = 1, **3** n = 2, **4** n = 3) have been prepared and characterised and are rare examples of luminescent 1,2,3-triazole-based osmium(II) complexes. For **3** we present an attractive and particularly mild preparative route *via* an osmium(II) η^6-arene precursor circumventing the harsh conditions that are usually required. Due to the high spin-orbit coupling constant associated with the Os(II) centre the absorption spectra of the complexes all display absorption bands of appreciable intensity in the range 500 – 700 nm corresponding to spin-forbidden ground-state-to-^{3}MLCT transitions, which occur at significantly lower energies than the corresponding spin-allowed ^{1}MLCT transitions. The homoleptic complex **4** is a bright emitter (λ_{max}^{em} = 614 nm) with a relatively high quantum yield of emission of ~ 40 % in deoxygenated acetonitrile solutions at RT. Water soluble chloride salts of **1**-**4** were also prepared, all of which remain emissive in aerated aqueous solutions at room temperature. The complexes were investigated for their potential as phosphorescent cellular imaging agents whereby efficient excitation into the ^{3}MLCT absorption bands at the red side of the visible range circumvents

autofluorescence from biological specimens which do not absorb in this region of the spectrum. Confocal microscopy reveals **4** to be readily taken up by cancer cell lines (HeLa and EJ) with apparent lysosomal and endosomal localisation, whilst toxicity assays reveal that the compounds have low dark and light toxicity. These complexes therefore provide an excellent platform for the development of efficient luminescent cellular imaging agents with advantageous photophysical properties which enable excitation and emission in the biologically transparent region of the optical spectrum.

Introduction

Over recent decades innumerable reports have appeared in the literature on kinetically inert complexes of d^6 transition metals such as Re(I), Ru(II) and Ir(III) detailing their extensive photophysical properties.[1] Of particular interest is the application of luminescent transition metal complexes as biocompatible probes for cellular imaging[2-7] which have recently become of interest for such applications alongside previously explored complexes of some p – and f-block elements.[8, 9] With d^6 complexes typically displaying long-lived triplet metal-to-ligand charge-transfer (^{3}MLCT) excited states from which phosphorescence occurs, time-gated techniques enable selective imaging of the transition metal complex probe without interference from background cellular autofluorescence.

Osmium(II) complexes exhibit significantly advantageous photophysical properties for biological imaging applications[10-13]; the high spin-orbit coupling constant associated with the osmium centre results in the usually spin-forbidden direct ground state to ^{3}MLCT state transitions to become of appreciable intensity in the UV-visible absorption spectra.[14, 15] These transitions occur at wavelengths significantly red-shifted relative to the corresponding spin-allowed transitions populating ^{1}MLCT states, and thus appear in the optimum window for the biologically transparent region. Emission from osmium(II)-based MLCT states typically occurs in the red to near-IR regions of the spectrum. These absorption and emission properties thus enable greater depth of tissue penetration for excitation (which can additionally be achieved at lower excitation energies thereby limiting tissue damage) and imaging of emission. Further, the ability to excite these complexes directly to the ^{3}MLCT state at longer wavelengths typically necessary for complexes of ruthenium(II), for example, aids the avoidance of autofluorescence from intrinsic biological chromophores, thus making imaging simpler and circumventing the need for time-gating techniques to achieve autofluorescence-free imaging.

Whilst there have been many examples of phosphorescent probes based on complexes of rhenium(I), ruthenium(II) and iridium(III) there have been only a handful of reports concerning the use of osmium(II) complexes for cellular imaging applications.[16-19] For example, Keyes and co-workers have reported a polyarginine-conjugated osmium(II) imidazophenanthroline complex for near-IR live-cell imaging applications.[20] Chao and co-workers recently reported a benzimidazolylpyridine-based osmium(II) complex which exhibited near-IR emission and lysosomal localisation upon cellular uptake.[21]

Recent years have seen a large number of reports concerning luminescent complexes of rhenium(I) and iridium(III) bearing 1,2,3-triazole-derived ligands[22, 23] with applications in light-emitting electrochemical cells and light-emitting diodes[24, 25] and biological imaging.[26-30] Osmium(II) complexes incorporating 1,2,3-triazole-based ligands are, on the other hand, rather rare.[31] There are only a few reported examples of luminescent dicationic osmium(II) complexes bearing neutral ligands incorporating a 5-membered heterocycle such as 1,2,4-triazoles.[32, 33] More commonly reported are charge-neutral complexes with anionic 1,2,4-triazolate or pyrazolate ligand systems which are frequently combined with phosphine, arsine or carbonyl donors.[34-38] We have recently reported a series of tris-bidentate triazole-based osmium(II) complexes and their application in light-emitting electrochemical cell devices[39, 40] and the bis-tridentate complex $[Os(btzpy)_2]^{2+}$ (btzpy = 2,6-bis(1-phenyl-1,2,3-triazol-4-yl)pyridine) which exhibits phosphorescence at 595 nm. This latter complex was shown to be readily taken up by HeLa and U2OS cancer cell lines and displays a high degree of mitochondrial localisation.[41]

The present work develops the area of Os(II) complexes with 1,2,3-triazole ligands and demonstrates the ability to systematically tune their photophysical properties. We present a systematic study on the coordination chemistry and photophysical properties of osmium(II) pytz complexes $[Os(bpy)_{3-n}(pytz)_n]^{2+}$ (**1** n = 0, **2** n = 1, **3** n = 2, **4** n = 3) and their application in live cell imaging. The bpy-containing complexes are emissive in the deep-red/near-IR whilst the homoleptic complex $[Os(pytz)_3]^{2+}$ is brightly emissive in the orange region of the spectrum. These attractive photophysical properties and our previous work led us to prepare water soluble chloride salts of these complexes and assess their potential in cellular imaging.

Results and Discussion

The complex $[Os(bpy)_2(pytz)][PF_6]_2$ (**2**) was prepared by adaptation of established procedures for the synthesis of heteroleptic osmium(II) complexes (Scheme 1).[39, 42] Briefly, $[Os(bpy)_2Cl_2]$ was heated under refluxing conditions in ethylene glycol with an equivalent of the pytz ligand. Subsequent counter-ion metathesis with ammonium hexafluorophosphate then enabled isolation of **2** as a dark green solid. As the pytz ligand is not symmetrical the two bpy ligands give rise to two separate sets of resonances in the ^{1}H NMR spectrum of **2**. The pyridyl triazole ligand exhibits a resonance for the triazole ring proton at δ 8.59, shifted downfield by 0.33 ppm relative to the corresponding resonance for the free ligand (δ 8.26 in CD_3CN).

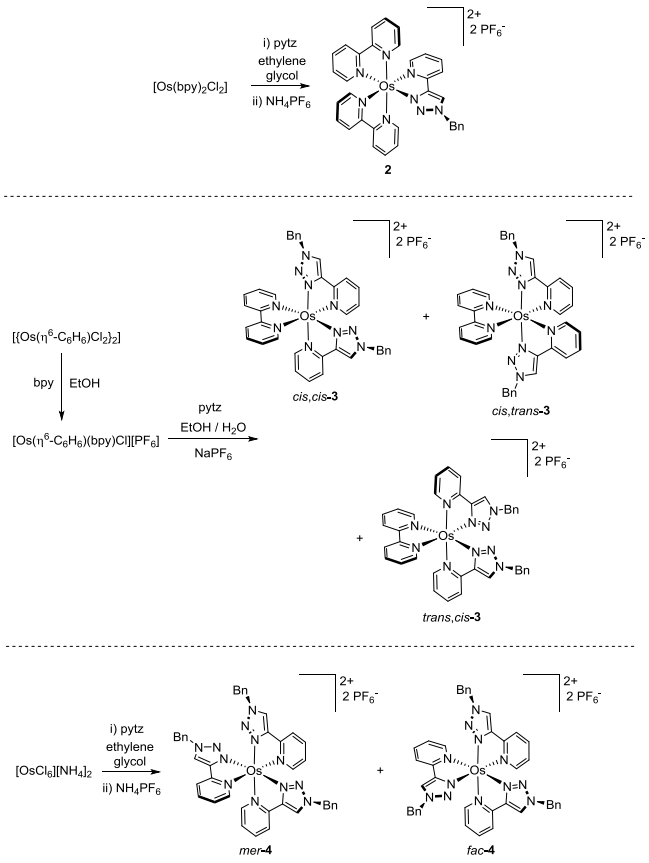

Scheme 1. Synthesis of $[Os(bpy)_2(pytz)][PF_6]_2$ (**2**), *cis*,*cis*-, *cis*,*trans*- and *trans*,*cis*-$[Os(bpy)(pytz)_2]^{2+}$ (*cis*,*cis*-**3**, *cis*,*trans*-**3** and *trans*,*cis*-**3)** and *mer*- and *fac*-$[Os(pytz)_3][PF_6]_2$ (*mer*-**4** and *fac*-**4**).

Crystals of X-ray diffraction quality were obtained for **2** and the molecular structure of the cation is depicted in Figure 1. The complex crystallises in the space group P21/n with a co-crystallised acetonitrile solvent molecule per osmium centre. The cation adopts a distorted octahedral geometry with unremarkable Os-N bond

lengths which vary from 2.02 to 2.09 Å. The bite angles of the three chelate ligands are very similar and are similarly unremarkable at approximately 78 °.

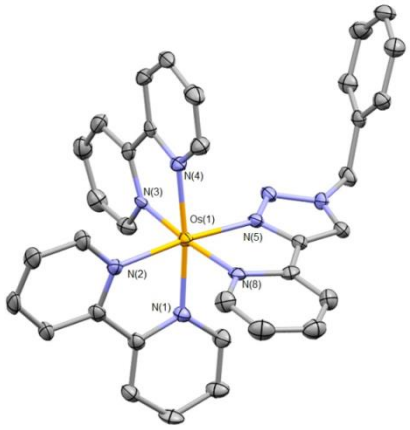

Figure 1. Molecular structure of the cation $[Os(bpy)_2(pytz)]^{2+}$ (ellipsoids at 50 % probability, hydrogen atoms, co-crystallised acetonitrile solvent molecule and hexafluorophosphate counterions removed for clarity). Selected bond lengths (Å) and angles (°): Os(1)-N(1) 2.058(4), Os(1)-N(2) 2.062(4), Os(1)-N(3) 2.042(5), Os(1)-N(4) 2.062(4), Os(1)-N(5) 2.024(4), Os(1)-N(8) 2.090(5), N(1)-Os(1)-N(2) 78.08(17), N(3)-Os(1)-N(4) 78.20(17), N(5)-Os(1)-N(8) 77.73(17), N(1)-Os(1)-N(4) 172.83(17), N(2)-Os(1)-N(5) 173.49(17), N(3)-Os(1)-N(8) 172.76(16). (Crystallographic information file: CCDC 1826209)

The complex $[Os(bpy)(pytz)_2][PF_6]_2$ (**3**) was prepared through a two-step procedure (Scheme 1), making use of a bipyridine-containing intermediate $[Os(\eta^6\text{-}C_6H_6)(bpy)Cl][PF_6]$, itself formed from the reaction between bpy and the chloro-bridged dimer $[\{Os(\eta^6\text{-}C_6H_6)Cl_2\}_2]$ as has been described elsewhere.[39] The pytz ligands were coordinated through reaction with $[Os(\eta^6\text{-}C_6H_6)(bpy)Cl][PF_6]$ in refluxing $EtOH/H_2O$, with the addition of NH_4PF_6 affording the final product as the hexafluorophosphate salt. As we have shown previously, as well as here, this osmium(II) arene route to heteroleptic complexes offers a significantly milder route as an alternative to the harsh conditions involving high boiling solvents normally associated with the synthesis of such materials. Due to the asymmetry of the pytz ligand, the complex is produced as a mixture of three isomers, *cis*,*cis*-**3**, *cis*,*trans*-**3** and *trans*,*cis*-**3** dependent on the respective regiochemistry of the pyridyl and triazole moieties of the two pytz ligands. Despite exhaustive efforts these isomers could not be satisfactorily separated by column or

preparative thin-layer chromatography. Subsequent results are therefore discussed based on analysis of **3** as a mixture of the three possible isomers.

The homoleptic complex $[Os(pytz)_3][PF_6]_2$ (**4**) was prepared by reaction of $(NH_4)_2OsCl_6$ with three equivalents of pytz in ethylene glycol under refluxing conditions followed by counter-ion metathesis. Due to the asymmetry of the pytz ligand the ^{1}H NMR spectrum of the initial product understandably shows signals for both meridional (*mer*-**4**) and facial (*fac*-**4**) isomers of **4** in an approximate 1:1.4 ratio (Figure 2). Separation of the two isomers proved extremely difficult, in contrast to the separation of the analogous ruthenium(II) system,[43] with both co-eluting in column chromatography with a wide range of solvent systems. However, successful separation was possible on a small scale by preparative thin-layer chromatography yielding very small quantities of each isomer, sufficient to allow spectroscopic characterisation.

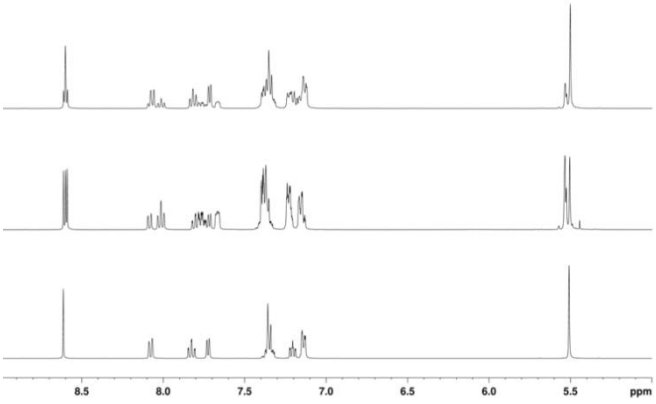

Figure 2. ^{1}H NMR spectra of **4** as a mixture of *fac* and *mer* isomers (top), *mer*-**4** (middle) and *fac*-**4** (bottom) in d_3-acetonitrile.

For *mer*-**4,** where the three pytz ligands are magnetically unique, three singlet resonances are observed at δ 8.59, 8.60 and 8.62 corresponding to the triazole ring protons (Figure 2). These are accompanied by resonances in the region δ 5.50-5.58 corresponding to the methylene protons of the benzyl substituents, one unique pair of which appears as a singlet at δ 5.50 displaying a strong nOe correlation signal with the proximal triazole ring proton at δ 8.60. Single crystals were grown for *mer*-**4** and the structure obtained. Whilst there is some residual electron density near to the metal that could not be satisfactorily modelled the data clearly shows the meridional arrangement of the pyridine and triazole rings of the pytz ligands. The structure is provided in the Supporting Information for reference (Figure S21).

The ^{1}H NMR spectrum of *fac*-**4** is much simpler than that of its meridional isomer due to the C_3 symmetry of the cation (Figure 2). A singlet resonance is observed at δ 8.61 for the triazole ring proton along with a resonance at δ 5.50 for the benzylic methylene protons. These are accompanied by four discrete signals for the pyridine rings, the most downfield of which (δ 8.07) is assigned to the H^3 position owing to the nOe correlation with the triazole ring proton. The resonances for the H^4, H^5 and H^6 positions give rise to signals centred at δ 7.82, 7.20 and 7.72 respectively as determined through COSY NMR analysis. The benzylic phenyl ring protons comprise the two remaining resonances at δ 7.14 and 7.31-7.40.

Complexes **1** and **2** together with the isomeric mixtures for complexes **3** and **4** were analysed by cyclic voltammetry (Figure 3) with electrochemical data summarised in Table 1. All complexes exhibit a reversible oxidation process centred between +0.44 and +0.46 V assigned to the Os(II)/Os(III) redox couple. The consistent oxidation potential across the series is indicative of a predominantly metal-centred HOMO. Complex **2** exhibits two reversible bpy-centred reductions at -1.71 and -1.94 V which are cathodically shifted relative to those observed for **1**, consistent with a destabilisation of the LUMO upon exchange of a bpy ligand for pytz. Likewise, the first reduction process observed for **3** is assigned to a bpy-centred process, with the further cathodic shift to -1.79 V again consistent with progressive destabilisation of the LUMO as more pytz ligands are included within the ligand set. An additional electrochemically quasi-reversible process is observed for **3** at -2.25 V, likely involving reduction of one of the pytz ligands. For **4**, only one quasi-reversible ligand-centred reduction is observed within the available electrochemical window at -2.11 V. The notable cathodic shift in this reduction potential of **4** relative to **1**-**3** is indicative of a significantly higher energy LUMO resulting from the necessary localisation of this orbital upon pytz rather than bpy.

Table 1. Electrochemical data for 1.5 mmol dm^{-3} MeCN solutions of complexes **1**-**4** measured at r.t. at a scan rate of 100 mVs^{-1}. Potentials are shown in V vs. Fc^+/Fc. Anodic-cathodic peak separations, $\Delta E_{a,c}$ are shown in mV within brackets ($\Delta E_{a,c}$ for Fc^+/Fc was typically 70 mV).

Complex	E_{ox} / V	E_{red} / V
1	0.44 (77)	-1.65 (67), -1.85 (76), -2.16 (76)
2	0.44 (71)	-1.71 (66), -1.94 (72)

3	0.45 (78)	-1.79 (85), -2.25 (97)
4	0.46 (72)	-2.11 (79)

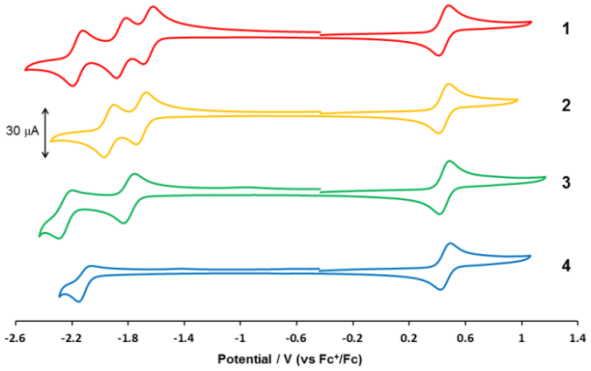

Figure 3. Cyclic voltammograms for 1.5 mmol dm^{-3} MeCN solutions of complexes **1**-**4** recorded at r.t. at 100 mVs^{-1}. Solutions contained 0.2 mol dm^{-3} NBu_4PF_6 as supporting electrolyte. All potentials are shown against the Fc^+/Fc couple.

The photophysical data for complexes **1** to **4** are summarised in Table 2. The UV-visible electronic absorption spectra of **1**-**3** in acetonitrile (Figure 4) exhibit a sharp and intense band at ~290 nm ascribed to singlet ligand-centred $\pi\rightarrow\pi^*$ transitions localised on bpy. This band is seen to decrease in intensity as bpy ligands are sequentially replaced by pytz, being accompanied by the rise in a new feature discernible at ~275 nm attributed to similar $\pi\rightarrow\pi^*$ transitions centred on the pytz ligands. In the visible region the complexes exhibit panchromatic absorption with moderately intense absorption bands between 330 and 520 nm in addition to absorptions of lower intensity at longer wavelength tailing off towards 700 nm. The more intense bands between 420 and 500 nm for **1** to **3** are assigned to spin-allowed ^{1}MLCT transitions to bipyridyl ligand(s) whereas the weaker and lower energy bands are assigned to spin-forbidden direct ^{3}MLCT transitions.[15] It is noted that these ^{1,3}MLCT bands for **2** and **3** are progressively blue shifted and reduce in intensity relative to those of **1** as the bpy-centred LUMO is destabilised upon substitution of bpy ligands for pytz. An increase in extinction coefficient observed for **3** between 330 and 420 nm is assigned to the contribution from ^{1}MLCT {Os-to-pytz} transitions. The spectra of *mer*-**4** and *fac*-**4** similarly feature absorption bands in the visible region assigned to both spin-allowed {Os-to-pytz} ^{1}MLCT (~350 to 430 nm) and spin-forbidden ^{3}MLCT transitions (~450 to 550 nm). However, since the LUMO of the pytz ligand is significantly destabilised relative to that of bpy these bands are significantly blue-

shifted compared to the absorption profiles of **1**-**3**. These data mirror the behaviour observed for related series of ruthenium(II) and osmium(II) triazole-containing complexes.[39, 44, 45]

Table 2. Summarised photophysical data for **1**-**3**, *mer*-**4** and *fac*-**4**.

Complex	λ^{abs} / nm[a]		λ^{em} / nm[a]	λ^{em} / nm[b]	τ / ns[a]	Φem / %[a,d]	Φem / %[c,d]	Φem / %[b,d]	Φ^1O_2 /%[e]
1	651, 585, 485, 451, 438, 390, 372, 331, 290, 254, 246	RT	732 [g]	736	38	0.5	0.8	0.3	26
		77 K [f]	706, 778[h]						
2	639, 575, 473, 432, 391, 363, 330, 289, 280, 242	RT	729 [g]	732	42	0.5	0.9	0.3	19
		77 K [f]	698, 765 [i]						
3	590, 459, 388, 355, 287, 275, 239	RT	716 [g]	718	53	0.7	1.3	0.4	32
		77 K [f]	683, 742 [i]						
mer-**4**	530, 485, 406, 380, 315, 274, 238	RT	613 [h]	-	50	1.3	47	-	-
		77 K [f]	568, 611 [i]						
fac-**4**	523, 488, 404, 379, 310, 274, 239	RT	615 [h]	-	50	1.2	40	-	-
		77 K [f]	576, 618[i]						
mer/fac-**4**				622	50 340[b] (692 [j])	-	-	2.9 (6.2 [j])	62

[a] Aerated MeCN. [b] chloride salt in aerated aqueous solution. [c] Deoxygenated MeCN. [d] Relative to $[Ru(bpy)_3][PF_6]_2$. Φ_{em} = 0.018 in aerated MeCN. Ref [46], [e] chloride salt in aerated MeCN solution, relative to perinaphthenone. [f] In 4:1 EtOH/MeOH glass. [g] λ_{ex} = 440 nm. [h] λ_{ex} = 520 nm. [i] λ_{ex} = 500 nm. [j] chloride salt in Argon equilibrated aqueous solution.

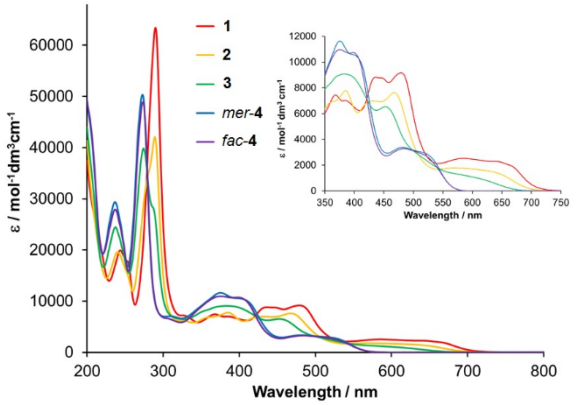

Figure 4. UV-visible electronic absorption spectra recorded for acetonitrile solutions of complexes **1**-**3**, *mer*-**4** and *fac*-**4** (inset: expansion of regions for ^{1}MLCT and ^{3}MLCT bands).

Complex **2** exhibits phosphorescence in aerated acetonitrile with a broad, featureless band in the red/near-infrared region of the spectrum (λ_{max} = 729 nm, Figure 5), attributed to an emissive state of ^{3}MLCT character. The emission is slightly blue-shifted relative to that of $[Os(bpy)_3]^{2+}$ (λ_{max} = 732 nm), with emission from **3** further shifted to higher energy (λ_{max} = 716 nm). This progressive trend due to destabilisation of the LUMO of the complex after replacement of the bpy ligands by pytz is in agreement with both UV-visible absorption and electrochemical data. Due to the appreciable intensity of the spin-forbidden ^{3}MLCT absorption bands excitation at wavelengths as long as 600 nm enable recording of emission spectra.

Emission spectra were also recorded for the isomerically pure homoleptic complexes *mer*-**4** and *fac*-**4**, with both showing near identical broad bands in the visible region (λ_{max} ~ 614 nm). The dramatic shift of emission maxima to higher energy compared to **1**-**3** again mirrors the large blue-shift in their absorption profiles.

Complexes **1** to **3** display short luminescence lifetimes (38 to 53 ns) and low emission quantum yields (0.5 to 0.7 %) in aerated acetonitrile solutions which obey the energy-gap law but are typical of dicationic bpy-based osmium(II) complexes[47] and those containing 1,2,4-triazole[32, 33] and -triazolate ligands.[48] The quantum yields increase to 0.8 to 1.3 % upon deoxygenating the solutions, in accordance with the triplet character of the emitting states. The homoleptic complexes *mer*-**4** and *fac*-**4** exhibit increased emission quantum yields relative to their bpy-containing heteroleptic analogues (1.2 – 1.3 %) which undergo dramatic enhancement on deoxygenating the solutions (47 and 40 % respectively). Approximate Stern-Volmer constants K_{SV} where estimated for each complex using the relations $I/I_0 = 1 + K_{SV}[O_2]$ where I and I_0 are the emission intensities at the given O_2 concentration and in deaerated solutions respectively. The data show that only moderate quenching of emission is observed for the bpy-containing complexes with $K_{SV} < 10$ atm^{-1}. However, the homoleptic complex **4** is found to exhibit far greater oxygen sensitivity with K_{SV} values of 83 and 86 atm^{-1} for the meridional and facial isomers respectively. These observations are consistent with the measured photoluminescence quantum yields.

Emission spectra recorded for **1**-**3**, *mer*-**4** and *fac*-**4** at 77 K in EtOH / MeOH glass matrices (Figure 5, bottom) display vibronic structure, are shifted to higher energy relative to the corresponding solution state spectra

due to rigidochromic effects, and exhibit the same trend in emission energy with increasing pytz content across the series as the emission spectra recorded in fluid solutions.

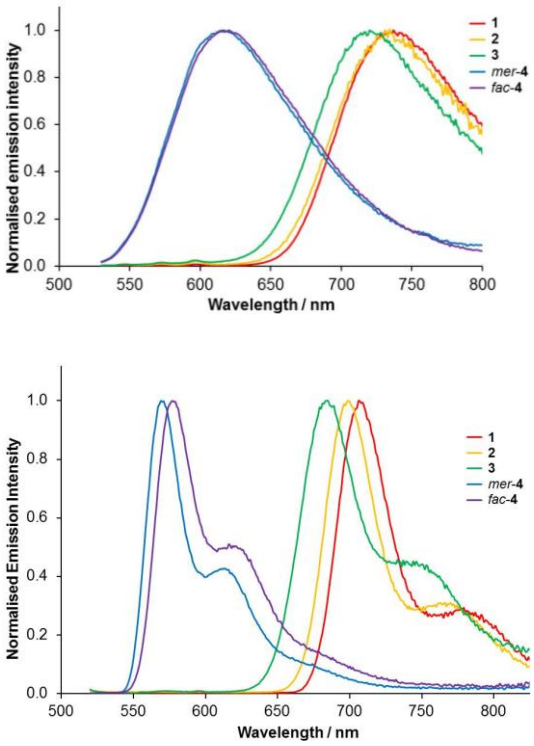

Figure 5. Top: Normalised emission spectra recorded for aerated MeCN solutions of **1**-**3**, *mer*-**4** and *fac*-**4** at r.t. Bottom: Low temperature emission spectra (77 K) for complexes **1**-**3**, *mer*-**4** and *fac*-**4** in a 4:1 EtOH:MeOH glass.

In order to obtain a deeper understanding of the photophysical properties of the complexes, density functional theory (DFT) calculations have been performed. The geometries of the cations for all possible linkage isomers of the complexes were calculated. In each case the benzyl substituents were simplified to methyl to reduce computational expense, since this replacement will have little impact on the photophysical properties. Representative plots of the HOMO and LUMO frontier orbitals are depicted in Figure 6 whilst computed energies of these orbitals and the energy gap between them are provided in Table 3. In each case the HOMO is of Os d_z^2 character whose energy is largely unaffected by the ligand set in agreement with the electrochemical data (*vide supra*). For the bpy-containing complexes **2** and **3** the LUMO is localised on the bpy ligands and is slightly

destabilised as the number of pytz ligands is increased. For **4** the LUMO is predominantly distributed over the pyridine rings of the three pytz ligands and is approximately 0.45 eV higher in energy compared to that of **2**, indicative of the significantly destabilised LUMO localised on the pytz ligand compared to that on the bpy ligand.

Time-dependent DFT (TDDFT) calculations were carried out in order to determine Frank-Condon excitation energies from the ground states to singlet excited states and thus simulate the optical absorption spectra of the complexes. Summarised data for selected transitions are provided in the Supporting Information. The energies of the more intense transitions in the calculated spectra align well with the experimental UV-visible absorption spectra for the complexes with a slight over-estimation of the energies. In all cases the S_1 states are of predominantly HOMO→LUMO ^{1}MLCT character but are of low oscillator strength ($f \leq 0.005$) and thus will contribute little to the experimentally observed absorption spectra. The first major transition for **2** occurs at 431 nm (S_5) and is of mixed HOMO-1→LUMO+1 and HOMO-2→LUMO ^{1}MLCT character where the excess electron density resides on the bpy ligands. For *cis,cis*-**3** and *cis,trans*-**3** comparable transitions are blue-shifted relative to that of **2** (419 nm (S_5) and 417 nm (S_5) respectively) in line with the experimentally determined optical absorption spectrum. For *trans,cis*-**3** a lesser blue-shift in the first intense transition (426 nm, S_3) is observed. These calculations for **2** and **3** also reveal that several transitions occur at higher energy (370-400 nm) that have ^{1}MLCT character with charge transfer to pytz. The lowest energy intense transitions for *fac*-**4** and *mer*-**4** appear at 393 nm (S_4) and 396 nm (S_4) respectively. These were determined to be of predominantly HOMO-1→LUMO and HOMO-2→LUMO ^{1}MLCT character respectively with localisation of the electron density in the excited state on the pytz ligands. The TDDFT data also confirmed assignments of the high energy intense bands below 300 nm as having ^{1}LC $\pi \rightarrow \pi^*$ character.

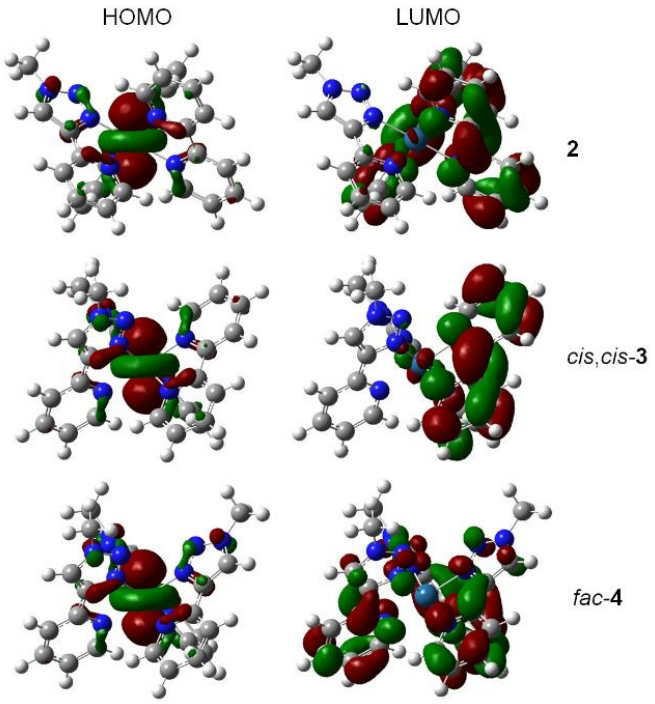

Figure 6. Representative plots of the HOMO and LUMO for **2**, *cis,cis*-**3** and *fac*-**4**.

Table 3. Calculated energies of HOMO and LUMO orbitals (eV) of complexes **1** to **4** and associated HOMO-LUMO gap.

Complex	HOMO	LUMO	HOMO - LUMO
2	-6.20	-2.67	3.53
cis,cis-**3**	-6.18	-2.57	3.61
cis,trans-**3**	-6.18	-2.53	3.65
trans,cis-**3**	-6.19	-2.60	3.58
mer-**4**	-6.17	-2.22	3.95
fac-**4**	-6.17	-2.21	3.96

Complexes **1**-**3**, *mer*-**4** and *fac*-**4** as their PF_6^- salts were subject to counter ion metathesis to yield the corresponding water soluble chloride salts. UV-visible absorption spectra recorded in water (Figure 7) closely resemble those of the corresponding hexafluorophosphate salts dissolved in acetonitrile (Figure 4, Table 2). The

chloride salts of the complexes remain emissive in aqueous solution, as can be seen from the spectra displayed in Figure 7 (bottom). The bpy-containing complexes show broad unstructured bands with slightly lower but comparable quantum yields to those of the hexafluorophosphate salts in acetonitrile. These bands are, however, slightly solvatochromically red-shifted with respect to the PF_6^- complexes in acetonitrile, consistent with the stabilisation of the emissive ^{3}MLCT states due to the greater polarity of the solvent. The quantum yields of singlet oxygen sensitised by the chloride salts of **1** to **4** in acetonitrile solutions were determined (Table 2). Modest quantum yields of between 19 and 32 % are observed for the bpy-containing complexes with a higher quantum yield of 62 % observed for **4** in agreement with the quenching data for the hexafluorophosphate salts.

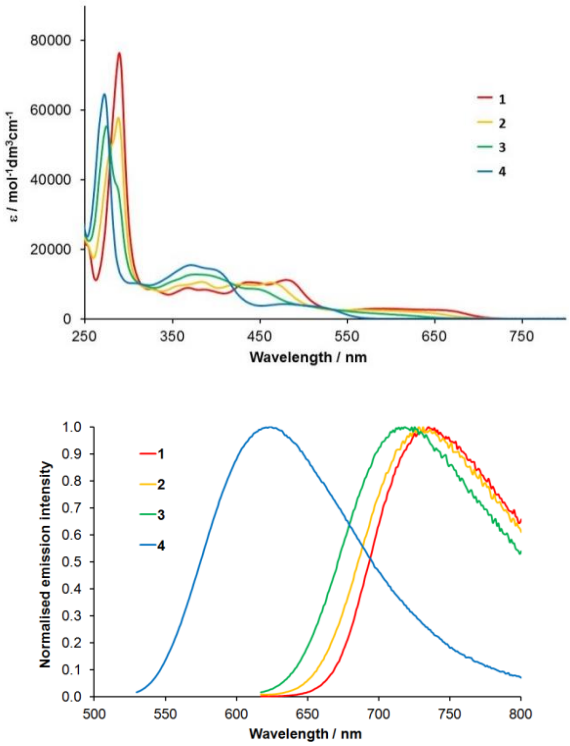

Figure 7. Top: UV-visible electronic absorption spectra recorded for complexes **1** to **4** as their chloride salts in aqueous solution. Bottom: Emission spectra for **1**-**4** in aerated aqueous solution at r.t. (for **1** to **3** λ^{ex} = 600 nm, for **4** λ^{ex} = 500 nm).

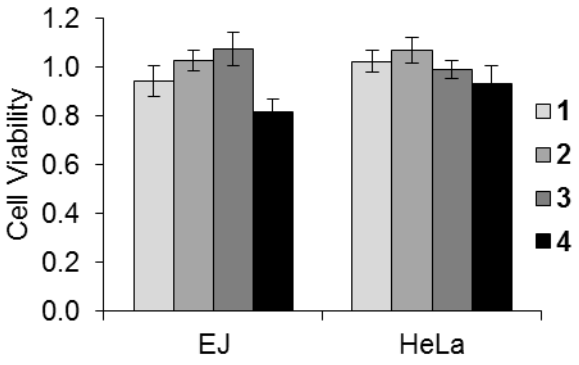

Figure 8. Dark viability MTT assay results for complexes **1** to **4** in EJ (bladder cancer) and HeLa (cervical cancer) cell lines following a 6 hour incubation with a 50 μM solution of the relevant complex.

Due to advantageous photophysical properties of the new Os(II) complexes as outlined above, we explored the potential of the complexes of these prototypical designs in preliminary confocal imaging studies. The cellular uptake, subcellular localisation and photo-induced cytotoxicity of complexes **1** to **4** as their water-soluble chloride salts were investigated in the EJ bladder cancer cell line and the HeLa cervical cancer cell line. Figure 8 shows dark toxicity as measured by MTT viability assay for **1** – **4.** To mimic imaging conditions, viability at 50 μM was measured immediately following a 6-hour incubation with each complex. In addition, to establish potential for therapeutic use, long-term viability was measured ~5 days after a 6 hour exposure to a higher dose of 100 μM (see Supporting Information Figure S19). These results indicate that the complexes have relatively low dark toxicity in both cell lines.

Confocal microscopy studies demonstrate that **4** enters cells, with only moderate cellular uptake of **3** being observed. Based on the lack of luminescence observed in the confocal microscopy experiments we conclude that **1** and **2** do not enter cells even following a 24 hour incubation (see Supporting Information Figure S18). Confocal images of **4** (20 μM) following a 6 hour incubation in the EJ bladder carcinoma cell line are presented in Figure 9. Localisation studies were hampered due to overlap of the absorption and emission bands of the probe with those of co-localisation stains and as such Pearson coefficients could not be reliably calculated. However, the emission shows cytoplasmic localisation with a distinct punctate pattern, which given the cationic

nature of the complexes is likely to be due to lysosomal and/or endosomal localisation. Similar localisation for **3** was observed (see Supporting Information Figure S18).

Whilst the complexes exhibit low dark toxicity (dark LD_{50} > 100 μM, Figure S19) the high degree of oxygen-based luminescence quenching and high singlet oxygen quantum yield for **4** raise the possibility for significant photocytotoxicity which would be a disadvantage for application in live-cell imaging. We therefore carried out preliminary experiments to assess any potential photocytotoxicity. Pleasingly, and somewhat unexpectedly, the utilisation of 3.6 J cm^{-2} 455 nm irradiation after incubation of cells with **3** and **4** (10 μM) demonstrated no photo-activated cytotoxicity (see supporting information Figure S20). Currently it is not clear why this lack of photo-induced toxicity is seen. One may tentatively speculate that the lack of photosensitising activity at relatively low doses (10 μM) may be indicative of intrinsically lower singlet oxygen generation in cytoplasmic media or that the generation of singlet oxygen at the site of localisation is far less damaging than when generated at, for example, the mitochondria or nucleus.[49] It could also be tentatively suggested that the observed localisation results in envelopment of the complex in lysosomal structures, thus shielding the complex from molecular oxygen and resulting in reduced quenching and efficient luminescent staining. Nevertheless, the complexes presented here therefore provide an excellent platform for the further development of luminescent cellular imaging agents.

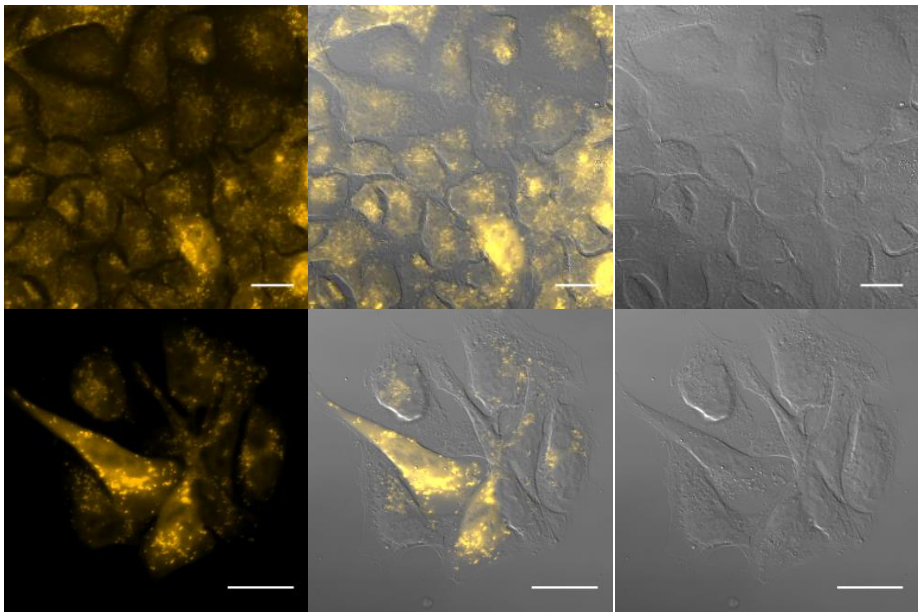

Figure 9. Confocal microscopy images of EJ bladder carcinoma cells incubated with complex **4** (20 μM, 6 hour incubation). Each panel comprises emission image (left, λ_{exc} = 543 nm, λ_{em} = 565-615 nm), bright-field image (right) and overlay of emission and bright-field images (centre). Scale bars = 20 μm.

Conclusions

The unique photophysical properties of osmium(II) complexes offer significant opportunities for biological imaging applications. The pyridyltriazole complexes reported here exhibit phosphorescence in the biologically transparent orange/red to deep red/near-IR region of the spectrum in aqueous solution (Cl-salts) or in acetonitrile solution (PF_6-salts) through low energy excitation into spin-forbidden direct ^{3}MLCT bands. The homoleptic tris(pyridyltriazole) complex **4** has been shown to be brightly emissive and undergoes cellular uptake in two cancer cell lines with likely lysosomal and endosomal localisation. Further development of this prototypical complex through variation of the structure of the triazole-based ligand could be envisaged to increase cellular uptake and to red-shift the absorption profile toward those of the heteroleptic complexes reported and thus provide an increased overlap with the optimum biological window. Modification of the bipyridyl substituents in the heteroleptic complexes may similarly result in improved cellular uptake for imaging in the deep-red region of the spectrum. The triazole complexes therefore present

an excellent platform for the development of non-toxic live-cell imaging probes which can be excited, and monitored, in the red region of the spectrum in the range of relative transparency of biological specimens.

Experimental Section

General Methods

$[Os(bpy)_3][PF_6]_2$,[42] $[Os(bpy)_2Cl_2]$,[42], $[\{Os(\eta^6\text{-}C_6H_6)Cl_2\}_2]$[50] $[Os(\eta^6\text{-}C_6H_6)(bpy)Cl][PF_6]$[39] and pytz[51] were prepared according to previously reported procedures. Ammonium hexachloroosmate(IV) was purchased from Alfa Aesar whilst all other reagents were purchased from Sigma-Aldrich, Acros Organics or Fluorochem and used as supplied. All synthetic manipulations were carried out under an atmosphere of dry N_2 employing standard Schlenk line techniques. Preparative thin layer chromatography was performed on silica plates (Analtech Uniplate) of size 20 x 20 cm and 1500 micron thickness. NMR spectra were recorded on Bruker Ascend 400 MHz and 500 MHz spectrometers, with all chemical shifts being quoted in ppm referenced relative to the residual solvent signal (MeCN, ^{1}H: δ 1.94, ^{13}C: δ 1.32, 118.26). High resolution mass spectrometry was performed on an Agilent 6210 TOF instrument with a dual ESI source. UV-visible absorption spectra were recorded on an Agilent Cary 60 spectrophotometer whilst emission spectra were recorded on a Fluoromax 4 spectrophotometer. Lifetime measurements were recorded by time-correlated single-photon counting using an Edinburgh Instruments Mini-Tau spectrometer. Cyclic voltammograms were measured using a PalmSens EmStat3 potentiostat with PSTrace electrochemical software (version 4.8). Analyte solutions (typical concentration 1.5 mmol dm^{-3}) were prepared using nitrogen saturated dry acetonitrile, freshly distilled from CaH_2. All measurements were conducted at room temperature under a stream of dry nitrogen at potential scan rates ranging from 50 to 500 mV s^{-1}. NBu_4PF_6 was used as a supporting electrolyte, being recrystallised from ethanol and oven dried prior to use, with a typical solution concentration of 0.2 mol dm^{-3}. The working electrode was glassy carbon, with platinum wire utilised as the counter electrode. The reference electrode was Ag/AgCl, being chemically isolated from the analyte solution by an electrolyte containing bridge tube tipped with a porous frit. Ferrocene was employed as an internal reference, with all potentials quoted relative to the Fc^+/Fc couple.

Synthesis of $[Os(bpy)_2(pytz)][PF_6]_2$ (2).

$[Os(bpy)_2Cl_2]$ (187 mg, 0.33 mmol) and pytz (80 mg, 0.34 mmol) were dissolved in ethylene glycol (10 ml) and refluxed under N_2 for 4 hrs. The resulting solution was allowed to cool to room temperature, treated with excess NH_4PF_6 (262 mg, 1.60 mmol) and stirred for a further hour. H_2O was added (10 ml) and the dark green precipitate collected by vacuum filtration and washed with cold water followed by diethyl ether. Purification was achieved *via* column chromatography (SiO_2, 4:1 CH_2Cl_2 / MeCN) with collection of the dark green coloured band and evaporation of the solvent. The resulting residue was subsequently re-dissolved in a small volume of 2 % MeOH / CH_2Cl_2 and passed through a short pad of alumina. Addition of excess hexane to the filtrate afforded the pure product as a dark green powder which was collected by filtration, washed with Et_2O and dried *in vacuo*. Yield = 100 mg, 30 %. ^{1}H NMR (CD_3CN, 400 MHz,): 5.47 (d, *J* = 15.0 Hz, 1H), 5.51 (d, *J* = 15.0 Hz, 1H), 7.11-7.27 (m, 4H), 7.28-7.43 (m, 6H), 7.52 (d, *J* = 5.6 Hz, 1H), 7.67 (d, *J* = 5.6 Hz, 1H), 7.72 (d, *J* = 5.5 Hz, 1H), 7.74-7.91 (m, 7H), 8.07 (d, *J* = 7.9 Hz, 1H), 8.37-8.46 (m, 2H), 8.49 (d, *J* = 8.2 Hz, 2H), 8.59 (s, 1H). ^{13}C NMR (101 MHz, CD_3CN): 56.47, 123.56, 124.61, 124.98, 125.38, 125.45, 127.15, 127.31, 128.18, 128.86, 128.91, 129.04, 129.18, 130.01, 130.10, 134.58, 137.91, 137.94, 137.96, 138.04, 138.60, 150.23, 151.87, 151.93, 152.24, 152.32, 152.43, 153.43, 159.96, 160.30, 160.36, 160.77. HRMS (ES); *m/z* calc. for $[OsC_{34}H_{28}N_8]^{2+}$: 370.1020, found: 370.1027. Anal. Calc. for $C_{34}H_{28}N_8P_2F_{12}Os$ (%): C 39.69, H 2.74, N 10.89, found (%): C 39.33, H 2.62, N 10.77.

Synthesis of *cis,cis*-, *cis,trans*-, *trans,cis*-$[Os(bpy)(pytz)_2][PF_6]_2$ (*cis,cis*-3, *cis,trans*-3, *trans,cis*-3).

$[Os(\eta^6\text{-}C_6H_6)(bpy)Cl][PF_6]$ (149 mg, 0.25 mmol), pytz (124 mg, 0.53 mmol) and $NaPF_6$ (100 mg, 0.59 mmol) were added to deaerated 3:1 (v/v) EtOH/H_2O (25 ml) and heated to 90 ^{o}C under an N_2 atmosphere for 48 hrs. The solution was allowed to cool to room temperature with the resulting precipitate collected by filtration and washed with H_2O followed by Et_2O. Purification was achieved *via* column chromatography (SiO_2, 2% MeOH / CH_2Cl_2), with the product eluting from a dark brown coloured band. Evaporation of the solvent to a minimum and addition of hexane precipitated the title complex as a brown coloured powder. Yield = 99 mg, 36 %. The product was obtained as a mixture of the *cis,cis*-; *cis,trans*-; and *trans,cis*- isomers which were not separated. ^{1}H NMR (CD_3CN, 400 MHz): 5.44-5.58 (m, 4H), 7.08-7.14 (m, 1H), 7.15-7.43 (m, 13 H), 7.59-7.67 (m, 2H), 7.73-7.90 (m, 6H), 8.03-8.11 (m, 2H), 8.35-8.46 (m, 2H), 8.56-8.63 (m, 2H). ^{13}C NMR (CD_3CN, 126 MHz): 56.36, 56.57, 123.19, 123.50, 123.56, 124.35, 124.56, 125.01, 126.45,

127.16, 127.18, 127.34, 128.04, 128.07, 128.79, 128.82, 129.20, 129.31, 129.93, 130.02, 130.05, 130.10, 130.12, 134.56, 134.73, 134.99, 137.77, 137.83, 137.95, 138.41, 138.44, 138.50, 150.20, 150.70, 150.95, 151.98, 152.24, 152.34, 152.41, 152.56, 153.03, 153.59, 153.83, 153.85, 160.76, 160.79, 160.97. HRMS (ES); *m/z* calc. for $[OsC_{38}H_{32}N_{10}]^{2+}$: 410.1208, found: 410.1209. Anal. Calc. for $C_{38}H_{32}N_{10}P_2F_{12}Os$ (%): Satisfactory elemental analysis could not be obtained for this compound.

Synthesis of *mer*- and *fac*-$[Os(pytz)_3][PF_6]_2$ (*mer*-4 and *fac*-4).

$[OsCl_6][NH_4]_2$ (202 mg, 0.46 mmol) and pytz (412 mg, 1.74 mmol) were dissolved in ethylene glycol (15 ml) and refluxed under N_2 for 2 hrs. The resulting solution was allowed to cool to room temperature, excess NH_4PF_6 (324 mg, 1.98 mmol) added and the mixture then stirred for a further 30 mins. H_2O (15 ml) was added and the dark orange precipitate then isolated by vacuum filtration, being washed with cold water followed by Et_2O. Purification was performed *via* column chromatography (SiO_2, 2% MeOH / CH_2Cl_2), with the product eluting from a bright red coloured band. Evaporation of the solvent to a minimum volume and addition of excess hexane precipitated the product as a red/orange coloured solid. Yield = 411 mg, 75 %. The product was found to be composed of a mixture of the meridonal and facial isomers in approximately a 1:1.4 respective ratio as estimated by ^{1}H NMR. Separation of these isomers was achieved through preparative thin layer chromatography (SiO_2, gradient elution, CH_2Cl_2 then 1:4 acetone/CH_2Cl_2) with the first orange coloured band containing exclusively the meridonal isomer. The facial isomer was obtained from the second (lower R_f) coloured band.

mer-$[Os(pytz)_3][PF_6]_2$: ^{1}H NMR (CD_3CN, 400 MHz): 5.50 (s, 2H), 5.52-5.58 (m, 4H), 7.12-7.19 (m, 4H), 7.20-7.27 (m, 5H), 7.32-7.44 (m, 9H), 7.65-7.69 (m, 2H), 7.70-7.84 (m, 4H), 7.99-8.04 (m, 2H), 8.08 (d, *J* = 7.9 Hz, 1H), 8.59 (s, 1H), 8.60 (s, 1H), 8.62 (s, 1H). ^{13}C NMR (CD_3CN, 126 MHz): 56.35, 56.58, 56.62, 122.58, 122.74, 123.46, 126.19, 126.40, 126.82, 127.13, 127.22, 128.88, 129.32, 129.34, 129.95, 130.07, 130.11, 130.13, 130.15, 134.61, 134.66, 135.00, 138.20, 138.27, 150.63, 151.01, 151.05, 152.56, 152.62, 153.08, 153.98, 154.23, 154.41.

fac-$[Os(pytz)_3][PF_6]_2$: ^{1}H NMR (CD_3CN, 400 MHz): 5.50 (s, 6 H), 7.14 (dd, *J* = 1.8, 7.6 Hz, 6H), 7.20 (ddd, *J* = 1.3, 5.9, 7.8 Hz, 3H), 7.31-7.40 (m, 9H), 7.72 (d, *J* = 5.6 Hz, 3H), 7.82 (td, *J* = 1.3, 7.8 Hz, 3H), 8.07 (d, *J* = 7.9 Hz, 3H), 8.61 (s, 3H). ^{13}C NMR (CD_3CN, 126 MHz): 56.42, 123.20, 126.49, 127.08, 128.88, 129.95, 130.12, 135.07, 138.42, 150.83, 152.46, 154.24.

HRMS (ES); *m/z* calc. for *mer/fac*-$[OsC_{42}H_{36}N_{12}]^{2+}$: 450.1395, found: 450.1406. Anal. Calc. for $C_{42}H_{36}N_{12}P_2F_{12}Os$ (%): C 42.43, H 3.05, N 14.14, found (%): C 42.21, H 2.97, N 13.97.

General procedure for the preparation of water soluble chloride salts.

The relevant Os complex as its hexafluorophosphate salt (100 mg) together with 2.5 weight equivalents of Amberlite chloride-form ion exchange resin (250 mg) were stirred in MeOH (25 ml) at room temperature in the dark for 24 h. The resin was removed by filtration and the filtrate evaporated to dryness. The residue was re-dissolved in the minimum volume of H_2O (< 10 ml) with subsequent freeze drying affording the relevant chloride salts as powders. Successful counter-ion metathesis was confirmed by the complete absence of resonances in ^{31}P and ^{19}F NMR spectra. (^{1}H NMR spectra for **1**-**4** as their chloride salts are presented within the ESI).

Computational Methods.

DFT calculations were carried out using the Gaussian 09 (Revision D.01) software package.[52] The complexes were optimised using the PBE0 functional[53] with the SDD effective core potential for osmium[54] and 6-311G* basis sets[55] for all other atoms. Solvation was modelled using the PCM solvent model for acetonitrile as implemented in Gaussian 09. The benzyl substituents of the experimentally investigated complexes were replaced by methyl for simplicity in the calculations. Minima were confirmed through vibrational frequency analysis. In some cases negative frequency modes were observed and corresponded to rotation of the methyl groups. Vertical excitation energies were determined through TDDFT calculations for the lowest energy 30 singlet roots to yield simulated optical absorption spectra.

Cell culture

Both cell lines HeLa (human cervical cancer) and EJ (human bladder carcinoma) were purchased from American Type Culture Collection–LGC partnership (Teddington, UK) and used within 20 passages of purchase. Cells were cultured using Dulbecco's modified Eagles Medium (DMEM) (Lonza, Cambridge UK) with 10% fetal calf serum (FCS) (Lonza, Cambridge UK) and cultured in an incubator (37 $^{\circ}$C, 5 % CO_2). The

cells were passaged when 70 – 80% confluency was reached and regularly checked for mycoplasma contamination.

Stock solutions of **1** – **4** were stored in deionised water at 10 mM, aliquoted in small volumes to avoid freeze/thaw cycles

Imaging

EJ cells were seeded on cover slips (22 x 22 mm, sterilised in industrial methylated spirits) placed in 6 well dishes at a density of ~2 x 10^5 per well and incubated overnight. Staining solutions of the desired compound were made by dilution into culture media and added to the cells for the desired time. Once incubation with the compounds had taken place the cells were washed (PBS x 3) and fixed (4% paraformaldehyde solution in PBS, 4 $^{\circ}$C, 20 mins) before being washed again (PBS x 3) and mounted (IMMU-MOUNT, Life Technologies Ltd, Paisley, UK).

The slides were imaged by confocal microscopy (Inverted Zeiss LSM 510 NLO microscope) using a 60 x lens with activation by helium-neon laser (λ = 543 nm). Emission was registered in the region 565-615 nm or 650-710 nm as specified.

Singlet oxygen yield measurement

The singlet oxygen yields Φ ($^1O_2$) of **1** – **4** were measured in air-equilibrated acetonitrile against the standard perinapthenone. The yields were determined by direct measurement of $^1O_2$ phosphorescence in the NIR (λ_{em} 1275 nm) with irradiation of the compounds at 355 nm by a pulsed Nd:YAG laser as described previously.[56]

MTT cell viability assay

Cells were seeded in 96-well plates (1 x 10^4 cells/well for short term and 1 x 10^3 cells/well for long term survival assays) and incubated overnight to adhere. **1** – **4** were added to the cells for 6 hours. Immediately (short term assay) or after ~5 days growth in fresh media (long term assay) thiazoyl blue (MTT) solution was added to each well (25 μL, 3 mg cm^{-3} in PBS). After a 3 hour incubation the media and MTT solution was removed from each well and DMSO was added (250 μL/well) and crystals dissolved. Optical density of wells at 540 nm was recorded on a plate reader (Multiskan fc, Thermo Fisher Scientific, Warrington, UK).

PDT

Cells were seeded in 6-well plates (2 x 10^4 cells/well) and allowed to adhere by incubation overnight. **4** was added to the cells for 6 hours. Following treatment, cells were washed (PBS) and trypsinized then re-suspended in PBS (2 ml) before each solution was divided. One half of each treatment concentration was kept in the dark while the other was treated with light (455 nm, 20 mW cm^{-2}, 3 mins, 3.6 J cm^{-2}) before cells were seeded at low density in 10 mm petri dishes (500 and 1000 cells/ dish) and left to form colonies (~10 days). Once colonies had formed the plates were washed (PBS) and stained (4 % methylene blue in 70 % methanol solution). Each colony is considered to represent a surviving cell with survival fractions calculated as number of surviving treated cells/ control cells.

Acknowledgements

The authors thank the State of Libya (SAEO), University of Huddersfield (PAS, PIPE, NJP), Yorkshire Cancer Research, Cancer Research UK, BBSRC, The Wellcome Trust, EPSRC Capital Equipment award, EPSRC KTA and the University of Sheffield (LKM, HEB, AJHMM & JAW) for supporting this work. Microscopy was performed on equipment purchased on the following grants: Wellcome Trust grant WT093134AIA and MRC SHIMA award MR/K015753/1. All calculations were performed on the ‘‘Sol’’ cluster of the Theoretical Chemistry Group of the University of Sheffield. We also thank Dr Jack Blackburn (University of Huddersfield) for assistance with mass spectrometry and elemental microanalysis.

Associated Content

Supporting Information

The supporting information is available on free of charge on the ACS publications website.

^{1}H NMR, ^{13}C NMR and high-resolution mass spectra for all complexes **1**-**4**, *mer*-**4** and *fac*-**4**.

Optimised ground state geometry atomic co-ordinates and TDDFT data for complexes **1**-**4**.

X-ray crystallographic data for **2** and *mer*-**4**.

Confocal microscopy images and cellular viability data for cells incubated with **1**-**4**.

Crystallographic Data

Crystallographic information files are available for complexes **2** (CCDC 1826209) and *mer*-**4** (CCDC 1850035).

References

1. Balzani, V.; Ceroni, P.; Juris, A. *Photochemistry and Photophysics: Concepts, Research, Applications*. Wiley-VCH: 2014.

2. Baggaley, E.; Botchway, S. W.; Haycock, J. W.; Morris, H.; Sazanovich, I. V.; Williams, J. A. G.; Weinstein, J. A. Long-lived metal complexes open up microsecond lifetime imaging microscopy under multiphoton excitation: From FLIM to PLIM and beyond. *Chem. Sci.* **2014,** *5*, 879-886.

3. Baggaley, E.; Weinstein, J. A.; Williams, J. A. G. Lighting the way to see inside the live cell with luminescent transition metal complexes. *Coord. Chem. Rev.* **2012,** *256*, 1762-1785.

4. Guo, Z.; Park, S.; Yoon, J.; Shin, I. Recent progress in the development of near-infrared fluorescent probes for bioimaging applications. *Chem. Soc. Rev.* **2014,** *43*, 16-29.

5. Lo, K. K. W. Luminescent Rhenium(I) and Iridium(III) Polypyridine Complexes as Biological Probes, Imaging Reagents, and Photocytotoxic Agents. *Acc. Chem. Res.* **2015,** *48*, 2985-2995.

6. Zhao, Q.; Huang, C.; Li, F. Phosphorescent heavy-metal complexes for bioimaging. *Chem. Soc. Rev.* **2011,** *40*, 2508-2524.

7. Tang, J.; Yin, H. Y.; Zhang, J. L. In *Inorganic and Organometallic Transition Metal Complexes with Biological Molecules and Living Cells*; Lo, K. K.-W., Ed.; Academic Press: 2017; pp 1-53.

8. Tang, J.; Yin, H.-Y.; Zhang, J.-L. A luminescent aluminium salen complex allows for monitoring dynamic vesicle trafficking from the Golgi apparatus to lysosomes in living cells. *Chem. Sci.* **2018,** *9*, 1931-1939.

9. Ning, Y.; Tang, J.; Liu, Y.-W.; Jing, J.; Sun, Y.; Zhang, J.-L. Highly luminescent, biocompatible ytterbium(iii) complexes as near-infrared fluorophores for living cell imaging. *Chem. Sci.* **2018,** *9*, 3742-3753.

10. Glazer, E. C. Panchromatic Osmium Complexes for Photodynamic Therapy: Solutions to Existing Problems and New Questions. *Photochem. Photobiol.* **2017,** *93*, 1326-1328.

11. Holmlin, R. E.; Stemp, E. D. A.; Barton, J. K. Os(phen)2dppz2+ in photoinduced dna-mediated electron transfer reactions. *J. Am. Chem. Soc.* **1996,** *118*, 5236-5244.

12. Holmlin, R. E.; Yao, J. A.; Barton, J. K. Dipyridophenazine complexes of Os(II) as red-emitting DNA probes: Synthesis, characterization, and photophysical properties. *Inorg. Chem.* **1999,** *38*, 174-189.

13. Lazic, S.; Kaspler, P.; Shi, G.; Monro, S.; Sainuddin, T.; Forward, S.; Kasimova, K.; Hennigar, R.; Mandel, A.; McFarland, S.; Lilge, L. Novel Osmium-based Coordination Complexes as Photosensitizers for Panchromatic Photodynamic Therapy. *Photochem. Photobiol.* **2017,** *93*, 1248-1258.

14. Ito, A.; Knight, T. E.; Stewart, D. J.; Brennaman, M. K.; Meyer, T. J. Rigid medium effects on photophysical properties of MLCT excited states of polypyridyl Os(II) complexes in polymerized poly(ethylene glycol)dimethacrylate monoliths. *J. Phys. Chem. A* **2014,** *118*, 10326-10332.

15. Kober, E. M.; Meyer, T. J. Concerning the absorption spectra of the ions M(bpy)32+ (M = Fe, Ru, Os; bpy = 2,2′-bipyridine). *Inorg. Chem.* **1982,** *21*, 3967-3977.

16. Alabau, R. G.; Esteruelas, M. A.; Oliván, M.; Oñate, E. Preparation of Phosphorescent Osmium(IV) Complexes with N,N′,C- and C,N,C′-Pincer Ligands. *Organometallics* **2017,** *36*, 1848-1859.

17. Chu, W. K.; Yiu, S. M.; Ko, C. C. Neutral luminescent Bis(bipyridyl) osmium(II) complexes with improved phosphorescent properties. *Organometallics* **2014,** *33*, 6771-6777.

18. Wang, J.; Sun, S.; Mu, D.; Wang, J.; Sun, W.; Xiong, X.; Qiao, B.; Peng, X. A Heterodinuclear Complex OsIr Exhibiting Near-Infrared Dual Luminescence Lights Up the Nucleoli of Living Cells. *Organometallics* **2014,** *33*, 2681-2684.

19. Yang, T.; Xia, A.; Liu, Q.; Shi, M.; Wu, H.; Xiong, L.; Huang, C.; Li, F. Polymer nanoparticles with an embedded phosphorescent osmium(ii) complex for cell imaging. *J. Mater. Chem.* **2011,** *21*, 5360-5367.

20. Byrne, A.; Dolan, C.; Moriarty, R. D.; Martin, A.; Neugebauer, U.; Forster, R. J.; Davies, A.; Volkov, Y.; Keyes, T. E. Osmium(II) polypyridyl polyarginine conjugate as a probe for live cell imaging; a comparison of uptake, localization and cytotoxicity with its ruthenium(II) analogue. *Dalton Trans.* **2015,** *44*, 14323-14332.

21. Zhang, P.; Wang, Y.; Qiu, K.; Zhao, Z.; Hu, R.; He, C.; Zhang, Q.; Chao, H. A NIR phosphorescent osmium(ii) complex as a lysosome tracking reagent and photodynamic therapeutic agent. *Chem. Commun.* **2017,** *53*, 12341-12344.

22. Scattergood, P. A.; Elliott, P. I. P. An unexpected journey from highly tunable phosphorescence to novel photochemistry of 1,2,3-triazole-based complexes. *Dalton Trans.* **2017,** *46*, 16343-16356.

23. Scattergood, P. A.; Sinopoli, A.; Elliott, P. I. P. Photophysics and photochemistry of 1,2,3-triazole-based complexes. *Coord. Chem. Rev.* **2017,** *350*, 136-154.

24. Fernández-Hernández, J. M.; Ladouceur, S.; Shen, Y.; Iordache, A.; Wang, X.; Donato, L.; Gallagher-Duval, S.; De Anda Villa, M.; Slinker, J. D.; De Cola, L.; Zysman-Colman, E. Blue light emitting electrochemical cells incorporating triazole-based luminophores. *J. Mater. Chem. C* **2013,** *1*, 7440-7452.

25. Orselli, E.; Albuquerque, R. Q.; Fransen, P. M.; Froehlich, R.; Janssen, H. M.; De Cola, L. 1,2,3-triazolyl-pyridine derivatives as chelating ligands for blue iridium(III) complexes. Photophysics and electroluminescent devices. *J. Mater. Chem.* **2008,** *18*, 4579-4590.

26. Clede, S.; Delsuc, N.; Laugel, C.; Lambert, F.; Sandt, C.; Baillet-Guffroy, A.; Policar, C. An easy-to-detect nona-arginine peptide for epidermal targeting. *Chem. Commun.* **2015,** *51*, 2687-2689.

27. Clède, S.; Lambert, F.; Saint-Fort, R.; Plamont, M.-A.; Bertrand, H.; Vessières, A.; Policar, C. Influence of the Side-Chain Length on the Cellular Uptake and the Cytotoxicity of Rhenium Triscarbonyl Derivatives: A Bimodal Infrared and Luminescence Quantitative Study. *Chem. Eur. J.* **2014,** *20*, 8714-8722.

28. Clede, S.; Lambert, F.; Sandt, C.; Gueroui, Z.; Refregiers, M.; Plamont, M.-A.; Dumas, P.; Vessieres, A.; Policar, C. A rhenium tris-carbonyl derivative as a single core multimodal probe for imaging (SCoMPI) combining infrared and luminescent properties. *Chem. Commun.* **2012,** *48*, 7729-7731.

29. Connell, T. U.; Hayne, D. J.; Ackermann, U.; Tochon-Danguy, H. J.; White, J. M.; Donnelly, P. S. Rhenium and technetium tricarbonyl complexes of 1,4-Substituted pyridyl-1,2,3-triazole bidentate 'click' ligands conjugated to a targeting RGD peptide. *J. Label. Compd. Radiopharm.* **2014,** *57*, 262-269.

30. Connell, T. U.; James, J. L.; White, A. R.; Donnelly, P. S. Protein Labelling with Versatile Phosphorescent Metal Complexes for Live Cell Luminescence Imaging. *Chem. Eur. J.* **2015,** *21*, 14146-14155.

31. Breul, A. M.; Rabelo De Moraes, I.; Menzel, R.; Pfeffer, M.; Winter, A.; Hager, M. D.; Rau, S.; Dietzek, B.; Beckert, R.; Schubert, U. S. Light-harvesting of polymerizable 4-hydroxy-1,3-thiazole monomers by energy transfer toward photoactive Os(ii) metal complexes in linear polymers. *Polym. Chem.* **2014,** *5*, 2715-2724.

32. Browne, W. R.; O'Connor, C. M.; Hughes, H. P.; Hage, R.; Walter, O.; Doering, M.; Gallagher, J. F.; Vos, J. G. Ruthenium(II) and osmium(II) polypyridyl complexes of an asymmetric pyrazinyl- and

pyridinyl-containing 1,2,4-triazole based ligand. Connectivity and physical properties of mononuclear complexes. *J. Chem. Soc. Dalton Trans.* **2002**, 4048-4054.

33. Giuffrida, G.; Calogero, G.; Guglielmo, G.; Ricevuto, V.; Ciano, M.; Campagna, S. Mono- and dinuclear complexes of ruthenium(II) and osmium(II) with a 3,5-bis(2-pyridyl)-1,2,4-triazole cyclohexyl-bridged spacer. Absorption spectra, luminescence properties, and electrochemical behavior. *Inorg. Chem.* **1993,** *32*, 1179-1183.

34. Tung, Y.-L.; Wu, P.-C.; Liu, C.-S.; Chi, Y.; Yu, J.-K.; Hu, Y.-H.; Chou, P.-T.; Peng, S.-M.; Lee, G.-H.; Tao, Y.; Carty, A. J.; Shu, C.-F.; Wu, F.-I. Highly Efficient Red Phosphorescent Osmium(II) Complexes for OLED Applications. *Organometallics* **2004,** *23*, 3745-3748.

35. Hsu, F.-C.; Tung, Y.-L.; Chi, Y.; Hsu, C.-C.; Cheng, Y.-M.; Ho, M.-L.; Chou, P.-T.; Peng, S.-M.; Carty, A. J. En Route to the Formation of High-Efficiency, Osmium(II)-Based Phosphorescent Materials. *Inorg. Chem.* **2006,** *45*, 10188-10196.

36. Liao, J.-L.; Chi, Y.; Liu, S.-H.; Lee, G.-H.; Chou, P.-T.; Huang, H.-X.; Su, Y.-D.; Chang, C.-H.; Lin, J.-S.; Tseng, M.-R. Os(II) Phosphors with Near-Infrared Emission Induced by Ligand-to-Ligand Charge Transfer Transition. *Inorg. Chem.* **2014,** *53*, 9366-9374.

37. Cheng, Y.-M.; Li, E. Y.; Lee, G.-H.; Chou, P.-T.; Lin, S.-Y.; Shu, C.-F.; Hwang, K.-C.; Chen, Y.-L.; Song, Y.-H.; Chi, Y. Strategic Design and Synthesis of Osmium(II) Complexes Bearing a Single Pyridyl Azolate π-Chromophore: Achieving High-Efficiency Blue Phosphorescence by Localized Excitation. *Inorg. Chem.* **2007,** *46*, 10276-10286.

38. Chang, S.-H.; Chang, C.-F.; Liao, J.-L.; Chi, Y.; Zhou, D.-Y.; Liao, L.-S.; Jiang, T.-Y.; Chou, T.-P.; Li, E. Y.; Lee, G.-H.; Kuo, T.-Y.; Chou, P.-T. Emissive Osmium(II) Complexes with Tetradentate Bis(pyridylpyrazolate) Chelates. *Inorg. Chem.* **2013,** *52*, 5867-5875.

39. Ross, D. A. W.; Scattergood, P. A.; Babaei, A.; Pertegás, A.; Bolink, H. J.; Elliott, P. I. P. Luminescent osmium(II) bi-1,2,3-triazol-4-yl complexes: Photophysical characterisation and application in light-emitting electrochemical cells. *Dalton Trans.* **2016,** *45*, 7748-7757.

40. Scattergood, P. A.; Ross, D. A. W.; Rice, C. R.; Elliott, P. I. P. Labilizing the Photoinert: Extraordinarily Facile Photochemical Ligand Ejection in an [Os(N^N)<inf>3</inf>]2+ Complex. *Angew. Chem. Int. Ed.* **2016,** *55*, 10697-10701.

41. Omar, S. A. E.; Scattergood, P. A.; McKenzie, L. K.; Bryant, H. E.; Weinstein, J. A.; Elliott, P. I. P. Towards Water Soluble Mitochondria-Targeting Theranostic Osmium(II) Triazole-Based Complexes. *Molecules* **2016,** *21*, 1382-1394.

42. Hamann, T. W.; Gstrein, F.; Brunschwig, B. S.; Lewis, N. S. Measurement of the free-energy dependence of interfacial charge-transfer rate constants using ZnO/H<inf>2</inf>O semiconductor/liquid contacts. *J. Am. Chem. Soc.* **2005,** *127*, 7815-7824.

43. Kumar, S. V.; Scottwell, S. O.; Waugh, E.; McAdam, C. J.; Hanton, L. R.; Brooks, H. J. L.; Crowley, J. D. Antimicrobial Properties of Tris(homoleptic) Ruthenium(II) 2-Pyridyl-1,2,3-triazole "click" Complexes against Pathogenic Bacteria, Including Methicillin-Resistant Staphylococcus aureus (MRSA). *Inorg. Chem.* **2016,** *55*, 9767-9777.

44. Happ, B.; Friebe, C.; Winter, A.; Hager, M. D.; Hoogenboom, R.; Schubert, U. S. 2-(1H-1,2,3-Triazol-4-yl)-Pyridine Ligands as Alternatives to 2,2 '-Bipyridines in Ruthenium(II) Complexes. *Chem. Asian. J.* **2009,** *4*, 154-163.

45. Welby, C. E.; Grkinic, S.; Zahid, A.; Uppal, B. S.; Gibson, E. A.; Rice, C. R.; Elliott, P. I. P. Synthesis, characterisation and theoretical study of ruthenium 4,4′-bi-1,2,3-triazolyl complexes: Fundamental switching of the nature of S 1 and T 1 states from MLCT to MC. *Dalton Trans.* **2012,** *41*, 7637-7646.

46. Suzuki, K.; Kobayashi, A.; Kaneko, S.; Takehira, K.; Yoshihara, T.; Ishida, H.; Shiina, Y.; Oishi, S.; Tobita, S. Reevaluation of absolute luminescence quantum yields of standard solutions using a spectrometer with an integrating sphere and a back-thinned CCD detector. *Phys. Chem. Chem. Phys.* **2009,** *11*, 9850-9860.

47. Kumaresan, D.; Shankar, K.; Vaidya, S.; Schmehl, R. H., Photochemistry and photophysics of coordination compounds: Osmium. In *Topics in Current Chemistry*, 2007; Vol. 281, pp 101-142.

48. Barigelletti, F.; De Cola, L.; Balzani, V.; Hage, R.; Haasnoot, J. G.; Reedijk, J.; Vos, J. G. Mononuclear and dinuclear osmium(II) compounds containing 2,2'-bipyridine and 3,5-bis(pyridin-2-yl)-1,2,4-triazole: synthesis, electrochemistry, absorption spectra, and luminescence properties. *Inorg. Chem.* **1991,** *30*, 641-645.

49. Zamora, A.; Vigueras, G.; Rodr ǵuez, V.; Santana, M. D.; Ruiz, J. Cyclometalated iridium(III) luminescent complexes in therapy and phototherapy. *Coord. Chem. Rev.* **2018,** *360*, 34-76.

50. Peacock, A. F. A.; Habtemariam, A.; Fernández, R.; Walland, V.; Fabbiani, F. P. A.; Parsons, S.; Aird, R. E.; Jodrell, D. I.; Sadler, P. J. Tuning the reactivity of osmium(II) and ruthenium(II) arene complexes under physiological conditions. *J. Am. Chem. Soc.* **2006,** *128*, 1739-1748.

51. Obata, M.; Kitamura, A.; Mori, A.; Kameyama, C.; Czaplewska, J. A.; Tanaka, R.; Kinoshita, I.; Kusumoto, T.; Hashimoto, H.; Harada, M.; Mikata, Y.; Funabiki, T.; Yano, S. Syntheses, structural characterization and photophysical properties of 4-(2-pyridyl)-1,2,3-triazole rhenium(I) complexes. *Dalton Trans.* **2008**, 3292-3300.

52. Frisch, M. J.; Trucks, G. W.; Schlegel, H. B.; Scuseria, G. E.; Robb, M. A.; Cheeseman, J. R.; Scalmani, G.; Barone, V.; Petersson, G. A.; Nakatsuji, H.; Li, X.; Caricato, M.; Marenich, A. V.; Bloino, J.; Janesko, B. G.; Gomperts, R.; Mennucci, B.; Hratchian, H. P.; Ortiz, J. V.; Izmaylov, A. F.; Sonnenberg, J. L.; Williams; Ding, F.; Lipparini, F.; Egidi, F.; Goings, J.; Peng, B.; Petrone, A.; Henderson, T.; Ranasinghe, D.; Zakrzewski, V. G.; Gao, J.; Rega, N.; Zheng, G.; Liang, W.; Hada, M.; Ehara, M.; Toyota, K.; Fukuda, R.; Hasegawa, J.; Ishida, M.; Nakajima, T.; Honda, Y.; Kitao, O.; Nakai, H.; Vreven, T.; Throssell, K.; Montgomery Jr., J. A.; Peralta, J. E.; Ogliaro, F.; Bearpark, M. J.; Heyd, J. J.; Brothers, E. N.; Kudin, K. N.; Staroverov, V. N.; Keith, T. A.; Kobayashi, R.; Normand, J.; Raghavachari, K.; Rendell, A. P.; Burant, J. C.; Iyengar, S. S.; Tomasi, J.; Cossi, M.; Millam, J. M.; Klene, M.; Adamo, C.; Cammi, R.; Ochterski, J. W.; Martin, R. L.; Morokuma, K.; Farkas, O.; Foresman, J. B.; Fox, D. J. *Gaussian 09 Rev. D.01*, Wallingford, CT, 2009.

53. Adamo, C.; Barone, V. Toward reliable density functional methods without adjustable parameters: The PBE0 model. *J. Chem. Phys.* **1999,** *110*, 6158-6170.

54. Andrae, D.; Häußermann, U.; Dolg, M.; Stoll, H.; Preuß, H. Energy-adjusted ab initio pseudopotentials for the second and third row transition elements. *Theo. Chim. Acta* **1990,** *77*, 123-141.

55. Krishnan, R.; Binkley, J. S.; Seeger, R.; Pople, J. A. Self-Consistent Molecular-Orbital Methods .20. Basis Set For Correlated Wave-Functions. *J. Chem. Phys.* **1980,** *72*, 650-654.

56. McKenzie, L. K.; Sazanovich, I. V.; Baggaley, E.; Bonneau, M.; Guerchais, V.; Williams, J. A. G.; Weinstein, J. A.; Bryant, H. E. Metal Complexes for Two-Photon Photodynamic Therapy: A Cyclometallated Iridium Complex Induces Two-Photon Photosensitization of Cancer Cells under Near-IR Light. *Chem. Eur. J.* **2017,** *23*, 234-238.

Table of Contents Entry

Salem A. E. Omar, Paul A. Scattergood, Luke K. McKenzie, Callum Jones, Nathan J. Patmore, Anthony J. H. M. Meijer, Julia A. Weinstein, Craig R. Rice, Helen E. Bryant and Paul I. P. Elliott

Synopsis

The synthesis and photophysical characterisation of new luminescent 1,2,3-triazole-containing osmium(II) complexes is presented along with results from their use in confocal imaging microscopy.